Evidence for Modified Gravity:

From Theory to Observation

By

Matthew Thomas Nichols

Submitted for Graduation with Honors

Department of Physics and Astronomy

College of Arts and Sciences

University of Louisville

May, 2012

ABSTRACT

One chief aim of modern cosmology is to explain the sudden acceleration of the expansion of the Universe over the most recent few billion years. Some believe the force needed to cause such a growth comes from a mysterious source called dark energy, which would have to comprise three-quarters of the energy density of the Universe in order to account for such force. Other astrophysicists believe the answers lie in the mathematical equations used to describe spacetime. Called modified gravity, this approach offers alternatives to traditional general relativity. This particular thesis is based on an $f(R)$ theory of gravity that includes a small alteration to the Einstein-Hilbert action used to derive the Einstein equations. Computer simulations using these theoretical models suggest unique changes when compared to traditional general relativity, including a discrepancy in galactic masses. When modified gravity is applied, new degrees of freedom arise from introduced scalar fields, creating a chameleon mechanism which allows matter to change its mass based on the local mass density of the region. The dynamical mass of a galaxy, determined through the velocity dispersion, is therefore affected and becomes dependent on the local matter density. While matter is affected by these new degrees of freedom, light is not. Due to the light-bending properties of lensing galaxies, the unaffected lensing mass of a galaxy can still be determined, even when modified gravity is assumed. When compared to each other, the lensing and dynamical masses of a single galaxy appear starkly different under modified gravity, making the lensing mass the perfect gauge from which to compare the effects of modified gravity. The goal of this pilot study is to determine the feasibility of measuring this mass difference, to compare it to the differences measured in computer simulations, and to search for any environmental dependence in the difference.

CONTENTS

1. INTRODUCTION

The buzz words "Dark Energy" prevail when it comes to explaining the sudden rapid expansion of the Universe discovered in the late 1990's [Riess et al. 1998]. The popular press readily prints that Albert Einstein had been right all along with his idea of a cosmological constant (now generally associated with dark energy) to explain why gravity had not pulled the Universe back together after the Big Bang like a giant rubber band [Lemonick 2011]. The idea of a mysterious force tearing the Universe apart has serious ramifications, including the possibility of adding new species of energy that can only be observed indirectly. Rather than continuing to look for evidence of a seemingly evasive force, a group of theorists decided to focus on the equations that describe the Universe. By modifying these equations, the theoreticians hope to better model the expansion of the Universe without the need to introduce new forms of energy. This is modified gravity: a mathematical manipulation of the fundamental equations that describe general relativity [Zhao et al. 2011a].

1.1 f(R) THEORIES

Modified gravity is a broad field encompassing many alternatives and alterations to general relativity. This project focuses on a brand referred to as $f(R)$ theories of gravity that create variations to the Einstein-Hilbert action. There are three main branches caused by assumptions made when deriving the Einstein equation using the variational principle. The version focused on in this thesis comes from the metric formalism and adds a relatively small alteration to the action. Having been called a toy theory for its simplicity, this simple form allows theorists to easily track the theory's divergence from general relativity while still maintaining a level of generality to predict the results of more complex modifications [Sotiriou & Valerio 2010].

The traditional Einstein-Hilbert action has the form [Sotiriou & Valerio 2010]:

$$S = -\frac{c^4}{16\pi G}\int \sqrt{-g}\, R d^4x \tag{1}$$

where c is the speed of light in vacuum, G is the gravitational constant, g is the determinant of the Friedmann-Robertson-Walker (FRW) metric, and R is the Ricci scalar, which can be thought of as a measure of deviation from flat Euclidian space. The FRW metric is an exact solution to the Einstein field equations which describe a homogeneous, isotropic universe. $f(R)$ theories force the action to become a function of the Ricci scalar [Sotiriou & Valerio 2010]:

$$S = -\frac{c^4}{16\pi G}\int \sqrt{-g}\, f(R) d^4x \tag{2}$$

Though visually a small change, the new function greatly impacts the derivation of the Einstein equations, as seen below. Through a variation of the original Einstein-Hilbert action, the traditional Einstein equation has the form [Hartle 2003]:

$$\boldsymbol{G}_{\mu\nu} = \frac{8\pi G}{c^4}\boldsymbol{T}_{\mu\nu} \tag{3}$$

where $\boldsymbol{G}_{\mu\nu}$ is the Einstein curvature tensor (measure of spacetime curvature) and $\boldsymbol{T}_{\mu\nu}$ is the stress-energy tensor (measure of matter energy density). Normally the Ricci scalar is tied up in the Einstein curvature tensor as a constant. Under modified gravity, the newly added function $f(R)$ adds a new term to the equation, such that [Zhao et al. 2011b]:

$$\boldsymbol{G}_{\mu\nu} + \boldsymbol{X}_{\mu\nu} = \frac{8\pi G}{c^4}\boldsymbol{T}_{\mu\nu} \tag{4}$$

where $\boldsymbol{X}_{\mu\nu}$ is the modification to general relativity. This term is given by [Zhao et al. 2011b]:

$$\boldsymbol{X}_{\mu\nu} = f'(R)R_{\mu\nu} - \left(\frac{1}{2}f(R) - \square f'(R)\right)g_{\mu\nu} - \nabla_\mu\nabla_\nu f'(R) \tag{5}$$

where $f'(R)$ is the first derivative of the function, $R_{\mu\nu}$ is the Ricci curvature, $g_{\mu\nu}$ refers to the metric, $\square$ is the d'Alembertian, and $\nabla_\mu\nabla_\nu$ is the covariant derivative. The exact solution to the Einstein equation is a line element that contains both time and spatial components. The standard cosmological model is considered to be the FRW metric, whose perturbed line element in the Newtonian gauge appears as [Zhao et al. 2011a]:

$$ds^2 = a^2(\eta)[(1+2\Phi)d\eta^2 - (1-2\Psi)dr^2] \tag{6}$$

where ds is the line element, Φ is the gravitational potential, Ψ is the spatial curvature perturbation, dr is the spatial component, and $a(\eta)$ is the scale factor which accounts for the expansion of the Universe.

Finding the time-time component of the modified Einstein equation gives a Poisson equation of the form [Zhao et al. 2011a]:

$$\nabla^2\Phi = 4\pi G a^2 \delta_{\rho\text{eff}} \tag{7}$$

where Φ is the gravitational potential, G is the gravitational constant, a is the scale factor, and $\delta_{\rho\text{eff}}$ is the effective energy density containing the modifications. This equation is crucial to understanding the reasons for how the research methods discussed later can be used to show the effects of $f(R)$ modifications. It can be shown that modified gravity affects potentials on the galactic scale. By measuring the masses of galaxies, it becomes possible to search for evidence of modified gravity.

1.2 EVIDENCE FROM GALAXY MASSES

There are two basic techniques for measuring the mass of a galaxy, both of which are described in further detail in later sections. The first method of determining the mass of a galaxy (called the dynamical mass) is by analyzing the total energy of the system. Gravitational potential energy is a function of mass, meaning that in modified gravity, the potential gained from Equation (7) is different than in traditional relativity due to the modifications in $\delta_{\rho\text{eff}}$. Therefore, the dynamical mass of a galaxy is changed when modified gravity is applied [Zhao et al. 2011a].

The second technique for measuring the mass of a galaxy involves a phenomenon known as gravitational lensing. Massive objects like galaxies bend spacetime and light around them, much as a lens refracts light. The amount light is bent is a function of the mass of this lensing galaxy. This amount is described by the lensing potential and given by [Zhao et al. 2011a]:

$$\Phi_L = \frac{1}{2}(\Phi + \Psi) \tag{8}$$

where Φ is the gravitational potential and Ψ is the spatial curvature perturbation. The lensing potential satisfies Equation (7), recovering the matter density predicted by traditional general relativity [Zhao et al. 2011a]. This means light curves are not affected by modified gravity and can be used as a standard from which to compare. As an analogy to a traditional science experiment, the lensing mass can be considered the control, with the dynamical mass as the experimentally determined value.

1.3 THE CHAMELEON MECHANISM

An integral aspect of this particular theory of $f(R)$ gravity is the inclusion of the chameleon mechanism. Making the Einstein-Hilbert action into a function of the Ricci scalar creates degrees of freedom in the new scalar field. The chameleon mechanism masks the effects of the modifications on the small scale, explaining why traditional, unmodified general relativity seems to work fine on and around Earth. As the scale increases to the galactic level, the effects of modification become more prominent [Khoury & Weltman 2004]. On the small scale, the surrounding environment is relatively dense. Defining an environment to encompass entire galaxy clusters requires the inclusion of the empty space in between, thus significantly lowering the density. For instance, the mass density of Earth is on the order of $5 \times 10^3\ \mathrm{kg/m^3}$, whereas the mass density of the Milky Way galaxy is on the order of $6 \times 10^{-18}\ \mathrm{kg/m^3}$ [Sparke & Gallagher 2007]. Thus, the chameleon mechanism is dependent upon on the mass density of a region. The chameleon becomes more prominent in dense regions to screen the effects in the scalar field.

Through the chameleon mechanism, the effects of modified gravity become dependent on the regional mass density. Returning to the lensing and dynamical masses, this also implies the difference between the masses is environmentally dependent. As the density decreases on the large scale, the dynamical mass increases, causing the mass difference to increase. Likewise, as the density increases, the mass difference decreases. According to recent computer simulations, the masses' percent difference could be as large as 30% in under-dense regions [Zhao et al. 2011a].

Testing for the difference between the lensing and dynamical masses, and checking for an environmental dependence of the difference offers the opportunity to test this $f(R)$ theory of gravity observationally. The rest of this thesis outlines the method used in this pilot study to test this theory, making use of data from the Sloan Digital Sky Survey Data Release 8. The following sections describe choosing a data set, finding the lensing and dynamical masses, determining the difference between these masses, and defining a neighborhood in which to test for environmental dependence. An analysis follows each section, describing potential errors and the significance of the findings. Finally, a conclusion summarizes the results, including ideas for the future.

2. GALAXY SELECTION

Knowing the methods used in calculating the masses of galaxies, it was necessary to choose a sample set of galaxies for which specific characteristics were known. The most limiting set of factors came from the determination of the lensing mass. In order to calculate this mass, the Einstein ring of the galaxy must be measureable, and the distance to the source galaxy must be known. The largest single set of galaxies found was contained in Bolton et al. 2008a that contained all of the necessary components. The Sloan Digital Sky Survey Data Release 8 (SDSS DR8) provided the rest of the information. SDSS is a multinational collaboration that seeks to survey over one quarter of the night sky. With a 2.5 meter telescope at Apache Point Observatory in New Mexico, the survey makes photometric and spectroscopic observations, including photography. Released in January, 2011, DR8 includes 50TB of information on nearly 500 million objects, including celestial coordinates, redshift, velocity dispersions, and more. The survey covers the u, g, r, i, and z spectral bands, detecting wavelengths between 300 and 900 nanometers [SDSS3.org]. SDSS is a natural choice due to the large amounts of data collected and the latest release of data having been just a few months prior to the beginning of this project. The galaxies from Bolton were cross-referenced with SDSS to exclude the luminous red galaxies, which are older galaxies at higher redshifts whose characteristics vary from those of the larger main type galaxies. This cut was done to consider only one type of galaxy for consistency. The final sample size included 44 galaxies.

3. LENSING MASS

As seen in Section 1, determination of the lensing mass is crucial to this project. The lensing mass offers an invariant gauge from which to measure the impact of modified gravity.

3.1 INTRODUCTION TO LENSING

The image of a rubber sheet being stretched by a solar system is a popular way of showing how the gravitational fields of massive objects distort the continuum surrounding them. Einstein postulated in his theories of relativity that these fields, when strong enough, could bend light around them. While light may appear to be bending to the outside observer, light continues to travel in a straight line relative to the curvature of the distorted coordinate system which lies next to the mass, thus preserving the need for light to propagate in a straight line. As light travels toward the object, the trajectory is bent inward and around the object, redirecting the light much as a traditional glass lens focuses light [Narayan & Bartlemann 2008]. Figure 1 below shows this behavior, where the blue dot is the observer, the red dot is the lens, the yellow dot is the source, and the green lines are the light rays.

FIGURE 1: EINSTEIN RINGS

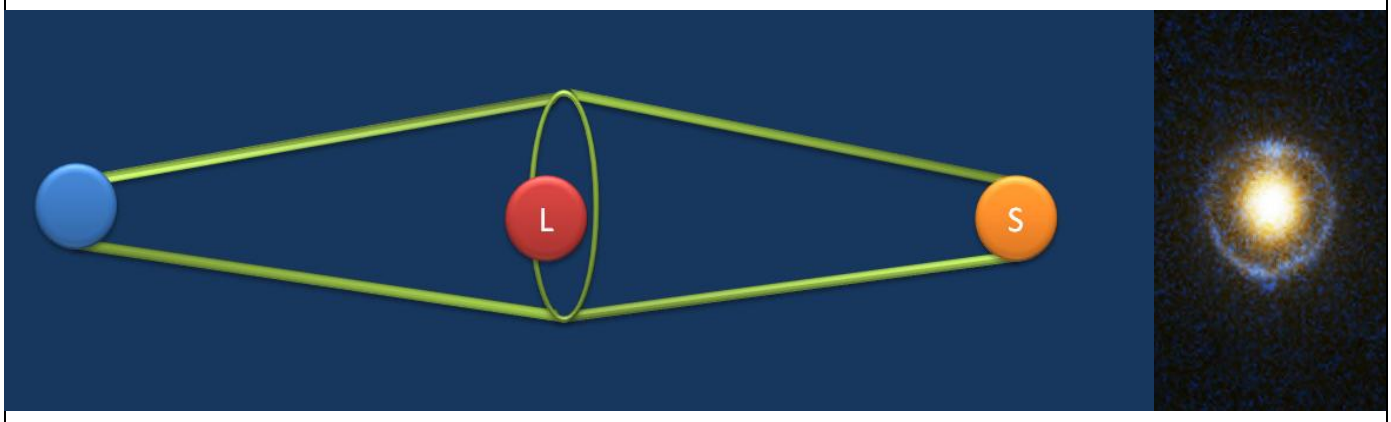

FIGURE 1: The diagram shows the ability of a galaxy (red dot) to bend the light from a far source, like another galaxy (yellow dot). Called gravitational lensing, it works much the same way as a traditional glass lens. The blue dot on the left represents the Earth. Assuming the three points are along the same line, if the observer and source are not located at the focal points of the lens, an Einstein ring will appear. Photo courtesy of National Aeronautics and Space Administration

A galaxy whose light has been gravitationally lensed will appear brighter on Earth than it would without the lens since more light from the galaxy is now reaching the observers. When Earth is not sitting at the focal point of the lensing system, a ring of light appears around the lensing galaxy, represented by the green circle in Figure 1. The radius of this ring is a function of the distances in the lensing system and the Schwarzschild radius, described below. Called the Einstein radius, it can be derived by a series of geometric approximations stemming from the lensing system found in Figure 2 [Hartle 2003].

FIGURE 2: GRAVITATIONAL LENSING

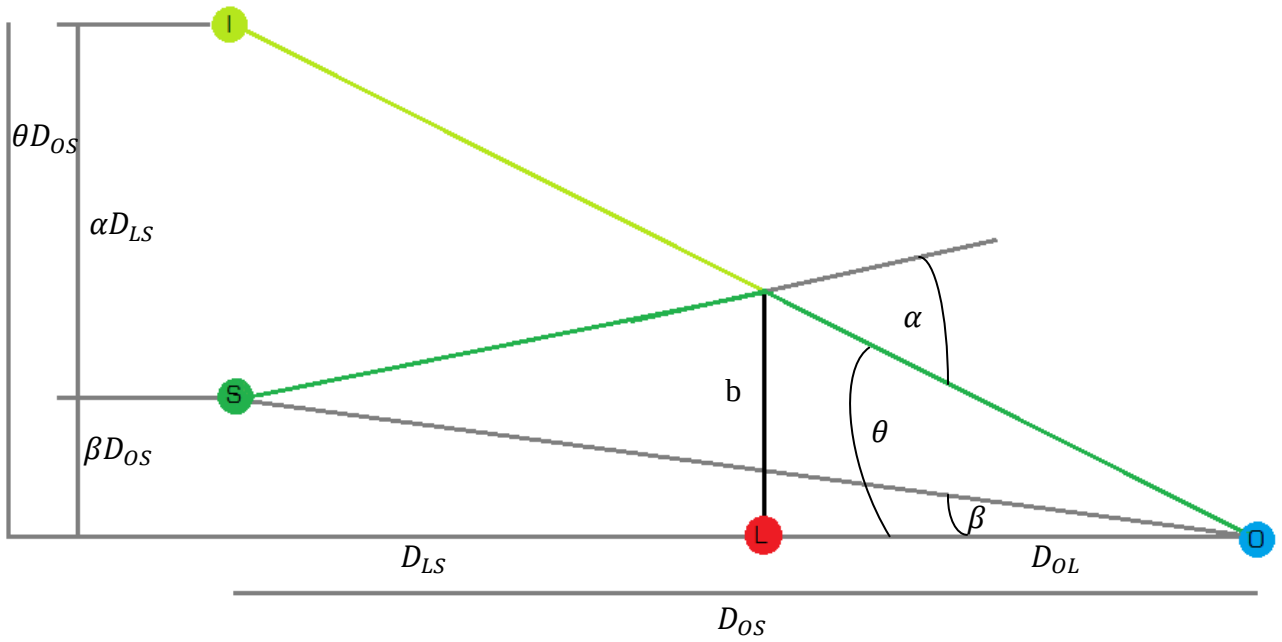

FIGURE 2: Massive objects have the ability to bend light. The blue O represents the observer, dark green S the source, light green I the image, and red L the lensing galaxy. D_x represents the angular diameter distance between the observer and lens (OL), observer and source (OS), and lens and source (LS). β is the angle between the axis and source, θ is the angle between the axis and image, and α is the angle the light ray is bent. The dark green line traces the path of light around the lensing galaxy, getting closest at a distance of b, the impact parameter.

In Figure 2, β is the angle between the horizontal axis and the source (S), θ is the angle to the image (I), and b is the point of closest approach to the lens (L) called the impact parameter. D_x represents the angular diameter distance (or the fraction of the actual size of the object compared

to its angular size seen from Earth) between observer and source (D_{OS}), observer and lens (D_{OL}), and lens and source (D_{LS}). Due to the small angles involved in gravitational lensing, distances perpendicular to the line of sight can be found by multiplying the angle times the corresponding distance, which leads to βD_{OS}, αD_{LS}, and θD_{OS}. By similarity, the impact parameter b can be approximated by θD_{OL}. The angle α represents the deflection angle of the light, which is proportional to the Schwarzschild radius. This angle is given by [Hartle 2003]:

$$\alpha = \frac{2}{b} R_S \tag{9}$$

where b is the impact parameter and R_S is the Schwarzschild radius. The Schwarzschild radius is the radius of a spherical object of mass M whose escape velocity is the speed of light. This means a particle would have to be travelling the speed of light in order to escape the gravitational pull of the mass. The Schwarzschild radius of the Sun is smaller than the actual diameter, which is why the Sun shines. A black hole, on the other hand, has a Schwarzschild radius larger than the actual diameter of the central mass, which explains why no light can escape. The equation for the Schwarzschild radius, which is derived from an object's gravitational potential is [Hartle 2003]:

$$R_S = \frac{2GM}{c^2} \tag{10}$$

where G is the gravitational constant, M is the mass of the object, and c is the speed of light. Returning to Figure 2, one can see the relationship between the distances perpendicular to the line of sight is [Hartle 2003]:

$$\theta D_{OS} = \beta D_{OS} + \alpha D_{LS} \tag{11}$$

With the newly approximated impact parameter substituted into Equation (9) for α and the assumption $\theta^2 \gg \beta\theta$ for perfect Einstein rings, the equation for the Einstein radius becomes [Hartle 2003]:

$$\theta_E = \left[2R_S \left(\frac{D_{LS}}{D_{OS} D_{OL}}\right)\right]^{1/2} \tag{12}$$

Substituting the Schwarzschild radius from Equation (10) and a little manipulation gives the final lensing mass [Bolton et al. 2008b]:

$$M_L = \frac{c^2 {\theta_E}^2}{4G} \frac{D_{OS} D_{OL}}{D_{LS}} \tag{13}$$

3.2 CALCULATING THE LENSING MASS

The necessary components for finding the lensing mass of the galaxies in the sample set come exclusively from tables found in Bolton et al. 2008a. In order to satisfy Equation (13), the spectroscopic redshifts for the source and lensing galaxies were converted to distances in meters using Ned Wright's Cosmological Calculator [Wright 2006]. Substituting the appropriate values into Equation (13) yields masses that range from 10^{10} to 10^{12} $M_\odot$ (Solar masses), which is comparable to most main type galaxies. Table 1 below shows the calculated lensing masses.

TABLE 1: CALCULATED LENSING MASSES

ID	Object ID	Lensing Mass ($M_\odot$)		ID	Object ID	Lensing Mass ($M_\odot$)
1	1237657189834621096	1.528E+11		23	1237661355931730052	1.353E+11
2	1237652947992838246	3.554E+11		24	1237654604261228656	2.033E+11
3	1237666340797153365	9.915E+10		25	1237658611984433262	3.084E+11
4	1237652901299814497	6.640E+11		26	1237658609296343089	1.622E+11
5	1237649963533926655	2.794E+10		27	1237661972796014740	1.860E+11
6	1237660957571940755	3.004E+11		28	1237671762641485915	2.286E+11
7	1237657630585585808	1.479E+11		29	1237651252040761551	3.449E+11
8	1237650796753322325	4.641E+11		30	1237648704589136004	1.148E+11
9	1237660669813129348	1.777E+11		31	1237655371441832114	4.021E+10
10	1237661065488761132	3.580E+11		32	1237661874024677506	7.090E+11
11	1237653663647727743	7.380E+10		33	1237674478123417869	1.268E+11
12	1237657632727302311	4.656E+11		34	1237654879128977672	6.771E+10
13	1237657874332385424	2.114E+11		35	1237655691403657326	9.408E+10
14	1237654601563373760	8.510E+10		36	1237655693018726805	3.183E+11
15	1237661355924586681	2.820E+11		37	1237654949985321081	1.031E+11
16	1237654605324550300	6.760E+10		38	1237661388689899825	3.712E+11

TABLE 1: CALCULATED LENSING MASSES cont.

ID	Object ID	Lensing Mass ($M_\odot$)		ID	Object ID	Lensing Mass ($M_\odot$)
17	1237657610723655845	1.245E+11		39	1237648672922862552	2.776E+11
18	1237657590318432374	1.122E+11		40	1237655130375586208	6.279E+11
19	1237658800422518913	9.857E+10		41	1237651715335127272	2.220E+11
20	1237655109449220224	1.439E+11		42	1237656495644541104	3.081E+11
21	1237658492814360790	2.033E+11		43	1237652900743938211	1.296E+11
22	1237671128051220497	2.124E+11		44	1237663784195326209	2.712E+11

TABLE 1: ID numbers refer to arbitrarily assigned identification numbers for ease of reference. Object ID refers to the identification number assigned by SDSS DR8. The lensing masses are calculated with Equation (13) using parameters provided by Bolton et al. 2008a. The masses are presented in $M_\odot$ (Solar masses).

3.3 LENSING MASS UNCERTAINTY

Determining the uncertainty in the lensing mass is a bit tricky due to the lack of established error values for the angular diameter distances, which are dependent upon spectroscopic redshift. Luckily, the SDSS database includes error values for the spectroscopic redshift. As with finding the actual angular diameter distances using Ned Wright's Cosmological Calculator [Wright 2006], the error in spectroscopic redshift can be transformed into a distance and treated as an approximation for the error of the angular diameter distance. To create a general absolute uncertainty in distance, the average spectroscopic redshift error was used in the Cosmological Calculator. The relative uncertainty of each distance was obtained by dividing the absolute error in distance by the corresponding average distance. The error for the Einstein angle was standardized at 2% by Bolton et al. 2008a. Table 2 below shows the associated errors found from averaged values of the components.

TABLE 2: LENSING MASS RELATIVE UNCERTAINTIES	
Einstein Angle: θ_E	0.02
Spectroscopic Redshift: z	0.0002047
Observer-Source Distance: D_{OS}	0.0002569
Observer-Lens Distance: D_{OL}	0.0001241
Lens-Source Distance: D_{LS}	0.0001542
Lensing Mass: M_L	0.028

TABLE 2: The relative uncertainty for the Einstein angle was a generalized uncertainty coming from Bolton et al. 2008a. The spectroscopic error was found in the SDSS DR8 database. The redshift error was used in the Cosmological Calculator to find a general absolute distance error. The relative uncertainties in distance were found by dividing by the absolute distance error by the average corresponding average distance. The final uncertainty is 2.8%

4. DYNAMICAL MASS

The second way to measure the mass of a galaxy is by analyzing the energy of the system. This so-called dynamical mass of a galaxy has been shown to vary under the conditions instituted by the modification term. Based on the chameleon mechanism, the magnitude of the dynamical mass is dependent upon the environmental matter density and could provide evidence for modified gravity.

4.1 INTRODUCTION TO DYNAMICAL MASSES

Analyzing the energy of a system involves a combination of the kinetic and potential energies. A form of the virial theorem, as seen below in Equation (14), provides a handy way of summing these two energies [Sparke & Gallagher 2007]:

$$2\langle T\rangle + \langle U\rangle = 0 \tag{14}$$

where $\langle T \rangle$ is the average kinetic energy over time and $\langle U \rangle$ is the average potential energy over time. When finding the energies of a galaxy, it is far more convenient to approach it as a uniformly dense sphere in a vacuum, sometimes referred to as a Plummer sphere in astrophysics. While usually the punch-line of a terrible physics joke, this approximation is appropriate given stellar dynamics and gravitational potential. The standard kinetic energy can be applied to the movements of the stars within the galaxy, with regular velocity replaced by velocity dispersion. The motion of stars around the center of a galaxy creates Doppler shifts in their spectra, revealing the stars' velocities. The velocity dispersion is related to the standard deviation of these velocities [Carroll & Ostlie 2007]. Therefore, the kinetic energy can be written as [Sparke & Gallagher 2007]:

$$T = 3\left(\frac{1}{2}m{\sigma_0}^2\right) \tag{15}$$

where m is the mass of the galaxy, σ_0 is the galaxy's velocity dispersion, and the factor of 3 out front represents the three spatial dimensions in which the galaxy's component stars are free to move. The potential energy term is a bit more complicated and begins with the standard two particle gravitational potential seen below:

$$U = -G\frac{M_1 M_2}{R} \tag{16}$$

where G is the gravitational constant, M_1 and M_2 are the masses of two particles, and R is the distance between them. Returning to the assumption that the galaxy is a sphere of uniform density, it becomes necessary to find the gravitational potential for a sphere. Using M_1 as the mass of the volume of a portion of the sphere at a radius of r, M_2 as a shell on the outside of the sphere with thickness dr, and dU as the sum of all of the potential energies for all of the shells, the equation for potential energy transforms into the following:

$$dU = -\frac{G}{r}\left(\frac{4}{3}\pi r^3\rho\right)(4\pi r^2\rho)dr \tag{17}$$

where r is the radius of the calculated volume and ρ is the constant density of the sphere. Evaluating this expression from the center of the sphere to the edge for $r = R$, and re-expressing

the density as the quotient of mass and volume returns the gravitational potential for a sphere of mass M and radius R in Equation (18) [Carroll & Ostlie 2007]:

$$U = -\frac{3}{5}\frac{GM^2}{R} \tag{18}$$

Plugging Equations (15) and (18) into Equation (14) and manipulating the equation reveals the galactic mass shown below in Equation (19) [Sparke & Gallagher 2007]:

$$M_D = \frac{5{\sigma_0}^2 R_{\text{eff}}}{G} \tag{19}$$

where M is the mass of the galaxy, σ_0 is the velocity dispersion, R_{eff} is the effective radius of the galaxy, and G is the gravitational constant. The effective radius of a galaxy is the radial distance at which half of the total light produced by the galaxy comes from inside the distance.

4.2 CALCULATING THE DYNAMICAL MASS

The necessary components for calculating the dynamical mass come from a combination of the tables found in Bolton et al. 2008a and SDSS DR8. The velocity dispersion and effective radius in arcseconds come from Bolton et al. 2008a. The effective radius is measured in arcseconds, but R is a physical distance. Replacing R with its geometric equivalent transforms Equation (19) into Equation (20):

$$M_D = \frac{5{\sigma_0}^2}{G} D_{OL} \tan(\gamma) \tag{20}$$

where γ is the effective radius in radians and D_{OL} is the angular diameter distance between the observer and the target galaxy. As with the lensing masses, the masses range from 10^{10} to 10^{12} $M_\odot$. The final calculated dynamical masses can be found in Table 3. These values are noticeably larger than the lensing mass values calculated in Section 3. Potential problems with accurately measuring the velocity dispersion and identifying galaxy type could explain this phenomenon, and are discussed more thoroughly in Section 5.

TABLE 3: CALCULATED DYNAMICAL MASSES

ID	Object ID	Dynamical Mass ($M_\odot$)		ID	Object ID	Dynamical Mass ($M_\odot$)
1	1237657189834621096	4.559E+11		23	1237661355931730052	1.8051E+11
2	1237652947992838246	6.352E+11		24	1237654604261228656	3.874E+11
3	1237666340797153365	5.314E+11		25	1237658611984433262	8.040E+11
4	1237652901299814497	1.569E+12		26	1237658609296343089	6.447E+11
5	1237649963533926655	5.909E+10		27	1237661972796014740	4.474E+11
6	1237660957571940755	5.153E+11		28	1237671762641485915	4.492E+11
7	1237657630585585808	4.458E+11		29	1237651252040761551	7.577E+11
8	1237650796753322325	1.413E+12		30	1237648704589136004	2.414E+11
9	1237660669813129348	4.483E+11		31	1237655371441832114	1.464E+11
10	1237661065488761132	6.593E+11		32	1237661874024677506	1.148E+12
11	1237653663647727743	1.062E+11		33	1237674478123417869	6.007E+11
12	1237657632727302311	1.032E+12		34	1237654879128977672	9.892E+10
13	1237657874332385424	4.859E+11		35	1237655691403657326	3.653E+11
14	1237654601563373760	1.515E+11		36	1237655693018726805	6.482E+11
15	1237661355924586681	3.656E+11		37	1237654949985321081	2.184E+11
16	1237654605324550300	1.519E+11		38	1237661388689899825	5.248E+11
17	1237657610723655845	1.967E+11		39	1237648672922862552	6.366E+11
18	1237657590318432374	2.227E+11		40	1237655130375586208	6.920E+11
19	1237658800422518913	2.442E+11		41	1237651715335127272	3.506E+11
20	1237655109449220224	3.619E+11		42	1237656495644541104	7.688E+11
21	1237658492814360790	3.814E+11		43	1237652900743938211	4.805E+11
22	1237671128051220497	9.264E+11		44	1237663784195326209	4.592E+11

TABLE 3: ID numbers refer to arbitrarily assigned identification numbers for ease of reference. Object ID refers to the identification number assigned by SDSS DR8. The lensing masses are calculated with Equation (20) using parameters provided by Bolton et al. 2008a. The masses are presented in $M_\odot$ (Solar masses).

4.3 DYNAMICAL MASS UNCERTAINTY

As with the lensing mass, there exists no established error for angular diameter distance. Once again, the error for this distance was approximated by using Ned Wright's Cosmological Calculator and the reported spectroscopic redshift error reported in SDSS DR8 [Wright 2006, SDSS3.org]. Bolton et al. 2008a also standardizes the errors for the effective radius and velocity dispersion at 3.5% and 7%, respectively. Averaged values were once again used to find relative error, with printed values seen in Table 4. The final uncertainty in the dynamical mass is 10.5%.

TABLE 4: DYNAMICAL MASS RELATIVE UNCERTAINTIES	
Velocity Dispersion: σ_0	0.07
Spectroscopic Redshift: z	0.0002047
Observer-Lens Distance: D_{OL}	0.0001241
Effective Radius: γ	0.035
Dynamical Mass: M_D	0.105

TABLE 4: The relative uncertainty for the velocity dispersion and effective radius come from Bolton et al. 2008a. As with the determination of the relative uncertainty in the lensing mass, the angular diameter distance error is found using the spectroscopic redshift uncertainty from SDSS DR8. The final uncertainty is 10.5%.

5. MASS DIFFERENCES

Returning to the theories of modified gravity, there should exist a difference between the lensing masses calculated in Section 3 and the dynamical masses calculated in Section 4 caused by the chameleon mechanism. According to Zhao et al. 2011a, the maximum allowed relative mass difference is 30%, which would appear on large galactic scales in low density regions. Table 5 shows a comparison of the masses, and indeed there exists a distinct difference between the lensing and dynamical masses.

TABLE 5: MASS DIFFERENCES					
ID	Object ID	Lensing Mass ($M_\odot$)	Dynamical Mass ($M_\odot$)	Mass Difference ($M_\odot$)	Percent Difference
1	1237657189834621096	1.528E+11	4.559E+11	3.03E+11	198.4%
2	1237652947992838246	3.554E+11	6.352E+11	2.80E+11	78.7%
3	1237666340797153365	9.915E+10	5.314E+11	4.32E+11	436.0%
4	1237652901299814497	6.640E+11	1.569E+12	9.05E+11	136.3%
5	1237649963533926655	2.794E+10	5.909E+10	3.12E+10	111.5%
6	1237660957571940755	3.004E+11	5.153E+11	2.15E+11	71.5%
7	1237657630585585808	1.479E+11	4.458E+11	2.98E+11	201.4%
8	1237650796753322325	4.641E+11	1.413E+12	9.49E+11	204.5%
9	1237660669813129348	1.777E+11	4.483E+11	2.71E+11	152.3%
10	1237661065488761132	3.580E+11	6.593E+11	3.01E+11	84.2%
11	1237653663647727743	7.380E+10	1.062E+11	3.24E+10	43.9%
12	1237657632727302311	4.656E+11	1.032E+12	5.66E+11	121.6%
13	1237657874332385424	2.114E+11	4.859E+11	2.75E+11	129.8%
14	1237654601563373760	8.510E+10	1.515E+11	6.64E+10	78.0%
15	1237661355924586681	2.820E+11	3.656E+11	8.36E+10	29.6%
16	1237654605324550300	6.760E+10	1.519E+11	8.43E+10	124.7%
17	1237657610723655845	1.245E+11	1.967E+11	7.22E+10	58.0%
18	1237657590318432374	1.122E+11	2.227E+11	1.11E+11	98.5%
19	1237658800422518913	9.857E+10	2.442E+11	1.46E+11	147.7%
20	1237655109449220224	1.439E+11	3.619E+11	2.18E+11	151.5%
21	1237658492814360790	2.033E+11	3.814E+11	1.78E+11	87.6%
22	1237671128051220497	2.124E+11	9.264E+11	7.14E+11	336.2%
23	1237661355931730052	1.353E+11	1.8051E+11	4.52E+10	33.4%
24	1237654604261228656	2.033E+11	3.874E+11	1.84E+11	90.6%
25	1237658611984433262	3.084E+11	8.040E+11	4.96E+11	160.7%
26	1237658609296343089	1.622E+11	6.447E+11	4.83E+11	297.5%
27	1237661972796014740	1.860E+11	4.474E+11	2.61E+11	140.5%
28	1237671762641485915	2.286E+11	4.492E+11	2.21E+11	96.5%
29	1237651252040761551	3.449E+11	7.577E+11	4.13E+11	119.7%
30	1237648704589136004	1.148E+11	2.414E+11	1.27E+11	110.3%
31	1237655371441832114	4.021E+10	1.464E+11	1.06E+11	264.1%
32	1237661874024677506	7.090E+11	1.148E+12	4.39E+11	61.9%
33	1237674478123417869	1.268E+11	6.007E+11	4.74E+11	373.7%

TABLE 5: MASS DIFFERENCES cont.

ID	Object ID	Lensing Mass ($M_\odot$)	Dynamical Mass ($M_\odot$)	Mass Difference ($M_\odot$)	Percent Difference
34	1237654879128977672	6.771E+10	9.892E+10	3.12E+10	46.1%
35	1237655691403657326	9.408E+10	3.653E+11	2.71E+11	288.3%
36	1237655693018726805	3.183E+11	6.482E+11	3.30E+11	103.6%
37	1237654949985321081	1.031E+11	2.184E+11	1.15E+11	111.8%
38	1237661388689899825	3.712E+11	5.248E+11	1.54E+11	41.4%
39	1237648672922862552	2.776E+11	6.366E+11	3.59E+11	129.3%
40	1237655130375586208	6.279E+11	6.920E+11	6.41E+10	10.2%
41	1237651715335127272	2.220E+11	3.506E+11	1.29E+11	57.9%
42	1237656495644541104	3.081E+11	7.688E+11	4.61E+11	149.5%
43	1237652900743938211	1.296E+11	4.805E+11	3.51E+11	270.8%
44	1237663784195326209	2.712E+11	4.592E+11	1.88E+11	69.3%

TABLE 5: The stark difference between the masses becomes immediately evident when looking at the percent difference. Treating the lensing and dynamical masses as the "theoretical" and "experimental" values in a standard science experiment, the percent difference skyrockets in some cases, going well beyond the 30% predicted by Zhao et al. 2011a. This could be caused by assumptions made in deriving the formula for the dynamical mass.

The percent difference was calculated by finding the quotient of the difference and the lensing mass. According to the theory, the lensing mass is unaltered by the addition of a modifying term to the Einstein-Hilbert action. This makes it the "theoretical" value with which to compare the dynamical mass, or "experimental" value. Zhao et al. 2011a predicted the difference to be a maximum of 30% of the lensing mass, a far cry from the percent differences found in Table 5. Even taking into account the uncertainties of calculating each mass does not rectify the enormous difference.

One possible explanation lies in the assumptions used when calculating the dynamical mass. While the method for approximating mass is correct, it typically works best for elliptical galaxies. Spiral galaxies behave differently, rotating quicker than their older elliptical cousins. Developing a new mass equation and positively identifying each individual galaxy may result in a more accurate depiction of the system. Looking at Bolton et al. 2008a reveals that four of the 44 galaxies were identified as late-type spiral galaxies. Further literature searches are required to

find a suitable replacement for the dynamical mass equation. Equation (20) includes the coefficient of 5 out front. Called the degree of virialization, this parameter is chosen based on the type of galaxy being analyzed. A smaller factor would yield a less drastic difference.

Velocity dispersions could also be a source of significant error. The orientation of the galaxy relative to the line of sight affects how well the velocity dispersion is measured. While the measurements may have been relatively precise, the accuracy may have been skewed due to the galaxy's orientation. Unfortunately the only way to correct this is to better understand the positioning of the galaxy when measuring the velocity dispersion.

Even though the percent difference in the masses was found to be far greater than predicted by Zhao et al. 2011a, it is still possible to search for an environmental dependence in the mass differences.

6. DEFINING A NEIGHBORHOOD

In order to determine if the difference between the lensing and dynamical masses is dependent upon the mass density of a region, it becomes necessary to define the volume of an environment, with the environment being defined as the region surrounding the lensing galaxy. Zhao et al. 2011a prescribes looking for the nearest neighbor of equal or greater mass as a measure of regional density. As the distance to the next massive neighbor decreases, the regional density increases. When comparing galactic masses in a computer simulation, this method seems sound; however, when attempted with observational data, the process becomes too involved for the scope of this project. Determining the masses of neighboring galaxies either requires a lensing system as previously described or velocity dispersions to obtain the dynamical mass. Unfortunately, not all galaxies have a source light behind them to show the effects of gravitational lensing. If the dynamical mass is truly environmentally dependent as theorized, then the dynamical masses would not serve as an independent measure, making this option for measuring mass impossible. This leaves few other options for finding the nearest neighbor using galactic masses.

6.1 CYLINDERS IN SPACE

The end goal is to measure the density, or mass contained within a volume. Taking a direct approach involves taking a number count of galaxies within a specified volume surrounding each target galaxy. If the volumes are equal for each galaxy, then a comparison can be made for each galactic neighborhood. Ideally, the volume would be spherically symmetric. Trying to model a sphere off axis in the spherical coordinate system used to map the Universe is difficult to achieve. This led to the use of cylindrical volumes around each target galaxy.

The cylinders were constructed by first drawing a circle of radius one megaparsec around the galaxy. Because distances in space transverse to the line of sight appear to vary based on how far from Earth they intersect the line of sight, it became necessary to calculate a different radius in arcseconds for each target galaxy. This involved using the angular diameter distance of the target galaxy to determine the number of arcminutes one megaparsec subtends at the galaxy's distance. Unfortunately, the angular diameter distances used previously in finding the masses were based on spectroscopic redshifts. When defining the environment, it is necessary to switch to a different measurement of redshift called the photometric redshift. Spectroscopic redshifts are determined by examining the emission and absorption lines of a galaxy and matching them to a known spectrum, yielding fairly accurate results. Photometric redshifts rely on information from the color filters to determine the redshift, which is less accurate than with spectroscopy. A quick glance at the difference shows as much as a 30% difference between the two. Even so, photometric redshifts are easier to take and are more available for fainter galaxies [SDSS3.org]. Within the SDSS database, not all objects have spectroscopic redshifts available, making the photometric redshift a mandatory component when searching for all neighbors.

Working with SDSS data, it also became easier and more efficient to obtain the angular diameter distance from the luminosity distance using the following relationship [Carroll and Ostlie 2007]:

$$D_{Lum} = D_{Ang}(1+z)^2 \tag{21}$$

where D_{Lum} is the luminosity distance, D_{Ang} is the angular diameter distance, and z is the photometric redshift. The luminosity distance is determined through the apparent and absolute

magnitudes (or relative and absolute brightness) of the galaxy. While luminosity distances are good when working with magnitudes and luminosities, the angular diameter distance is closer to the true physical distance to the galaxy. Obtaining this distance requires a bit more work than before, but using this method of determining the angular diameter distance standardizes the parameters used when defining an environment. This ensures better results in the end since all values are calculated from the same components.

The length of the cylinder was made using the newly recalculated angular diameter distance such that the diameter and length were equal. Because the lengths are measured radially from Earth, the cylindrical shapes are technically conical sections. This approximation is acceptable since the redshifts of the sample galaxies are similar to each other, making the cylindrical volumes nearly identical.

6.2 NEIGHBORS YOU CAN COUNT ON

Within each of these cylinders, the total number of known galaxies was tallied. At first glance, the galactic population is redshift-dependent, meaning that as the redshift increased, fewer galaxies were found in each volume. This is due to the galaxies' apparent magnitudes, which are a function of their brightness and distance away from Earth. Two galaxies that are equally bright will have very different apparent magnitudes if one is much farther away from the observer than the other. Telescopes have limitations on the amount of light they can gather, which means a galaxy that is far away may not be detected, while its identical twin many parsecs closer is detectable. Thus, the cylinders surrounding galaxies closer to Earth have more detectable neighbors than those regions further away. Correcting for this requires a magnitude cut to screen out faint galaxies detectable in near neighborhoods, but invisible in farther regions. To accomplish this, all neighbor galaxies included in the population count must have an absolute magnitude brighter than the dimmest galaxy detectable in the highest redshift cylinder, where the absolute magnitude of an object is a standard set as the apparent magnitude at a distance of 10 parsecs away. An approximation for the absolute magnitude of objects at low redshift requires the following [SDSS3.org]:

$$M_r = m_r - 5\log(4.28 \times 10^8 \times z) + 5 \quad (22)$$

where M_r is the absolute magnitude, m_r is the apparent magnitude, and z is the photometric redshift. With the magnitude system, brighter objects have a more negative value. SDSS reports an apparent magnitude limit of 22.2 [SDSS3.org]. The farthest galaxy in the sample has a redshift of 0.34. Therefore, the only objects within the region counted toward the population must have an absolute magnitude value more negative than -13.6.

Creating a single cylinder around each galaxy has the disadvantage of excluding galaxies that may only be partially contained within the region. By creating nested cylinders increasing volume, the mass density of the region becomes clearer. If the galaxy is sitting inside of a tightly packed cluster for instance, the interior cylinders will affect the population count more than the outer cylinders. These environmental divisions can be seen more clearly in Figure 3.

FIGURE 3: CYLINDRICAL VOLUMES

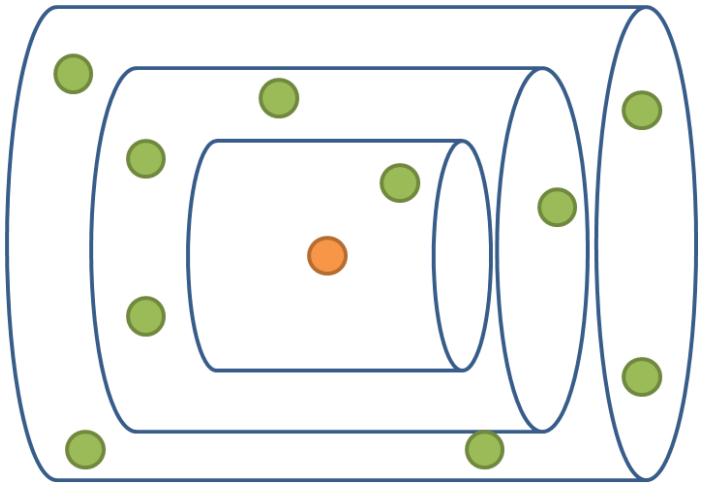

FIGURE 3: This image is a graphical representation of the cylinders used to define regions around each of the sample galaxies, represented by the orange dot. Cylinders with equal length and diameter are drawn around each galaxy, and a count of the number of galaxies is made. This helps determine the density of the environment in which the target galaxies reside. Nesting the cylinders helps deal with galaxies that are only partially in the defined volume. This nesting technique can also yield more information about where a galaxy sits relative to most of its neighbors.

Cutting into the ends of the cylinders like a pie and dividing it into quadrants allows for the determination of where the galaxy sits relative to the rest of its galactic neighbors. Looking at this information can indicate if the galaxy is symmetrically surrounded, or if a large portion of the mass lies off to one side. This information would be useful in future studies where additional information would help define the environment more accurately.

The final galaxy counts and population densities are seen in Table 6. For brevity, the cylinders represented have increasing radii of 2Mpc to show the increased number count over distance.

TABLE 6: POPULATION DENSITIES

ID	Object ID	2Mpc		6Mpc		10Mpc	
		Population	Density	Population	Density	Population	Density
1	1237657189834621096	1	0.1592	15	0.0884	74	0.0942
2	1237652947992838246	0	0.0000	7	0.0413	47	0.0598
3	1237666340797153365	2	0.3183	16	0.0943	77	0.0980
4	1237652901299814497	0	0.0000	15	0.0884	77	0.0980
5	1237649963533926655	1	0.1592	6	0.0354	30	0.0382
6	1237660957571940755	0	0.0000	7	0.0413	45	0.0573
7	1237657630585585808	0	0.0000	12	0.0707	49	0.0624
8	1237650796753322325	1	0.1592	19	0.1120	71	0.0904
9	1237660669813129348	1	0.1592	14	0.0825	63	0.0802
10	1237661065488761132	1	0.1592	13	0.0766	69	0.0879
11	1237653663647727743	0	0.0000	6	0.0354	43	0.0547
12	1237657632727302311	1	0.1592	13	0.0766	61	0.0777
13	1237657874332385424	1	0.1592	13	0.0766	47	0.0598
14	1237654601563373760	0	0.0000	13	0.0766	52	0.0662
15	1237661355924586681	1	0.1592	16	0.0943	53	0.0675
16	1237654605324550300	1	0.1592	17	0.1002	62	0.0789
17	1237657610723655845	1	0.1592	20	0.1179	102	0.1299
18	1237657590318432374	1	0.1592	17	0.1002	75	0.0955
19	1237658800422518913	0	0.0000	5	0.0295	35	0.0446
20	1237655109449220224	1	0.1592	22	0.1297	76	0.0968
21	1237658492814360790	0	0.0000	9	0.0531	58	0.0738

TABLE 6: POPULATION DENSITIES cont.

ID	Object ID	2Mpc		6Mpc		10Mpc	
		Population	Density	Population	Population	Density	Population
22	1237671128051220497	1	0.1592	18	0.1061	68	0.0866
23	1237661355931730052	0	0.0000	17	0.1002	55	0.0700
24	1237654604261228656	2	0.3183	26	0.1533	76	0.0968
25	1237658611984433262	0	0.0000	12	0.0707	58	0.0738
26	1237658609296343089	0	0.0000	6	0.0354	46	0.0586
27	1237661972796014740	0	0.0000	18	0.1061	59	0.0751
28	1237671762641485915	1	0.1592	10	0.0589	61	0.0777
29	1237651252040761551	0	0.0000	14	0.0825	62	0.0789
30	1237648704589136004	1	0.1592	20	0.1179	65	0.0828
31	1237655371441832114	0	0.0000	13	0.0766	41	0.0522
32	1237661874024677506	2	0.3183	16	0.0943	81	0.1031
33	1237674478123417869	1	0.1592	16	0.0943	66	0.0840
34	1237654879128977672	2	0.3183	7	0.0413	34	0.0433
35	1237655691403657326	0	0.0000	6	0.0354	22	0.0280
36	1237655693018726805	0	0.0000	13	0.0766	53	0.0675
37	1237654949985321081	0	0.0000	11	0.0648	51	0.0649
38	1237661388689899825	1	0.1592	17	0.1002	58	0.0738
39	1237648672922862552	1	0.1592	13	0.0766	46	0.0586
40	1237655130375586208	3	0.4775	15	0.0884	61	0.0777
41	1237651715335127272	0	0.0000	15	0.0884	68	0.0866
42	1237656495644541104	0	0.0000	9	0.0531	61	0.0777
43	1237652900743938211	0	0.0000	6	0.0354	42	0.0535
44	1237663784195326209	1	0.1592	14	0.0825	51	0.0649

TABLE 6: This table shows the number of galaxies counted within three cylindrical volumes surrounding each target galaxy. The cylinders in this table are of diameter and length 2Mpc, 6Mpc, and 10Mpc. The density is simply the quotient of the population count and the volume and is measured in galaxies per cubic megaparsec.

Examples of sample galaxy neighborhoods are seen in Figure 4.

FIGURE 4: GALACTIC NEIGHBORHOODS

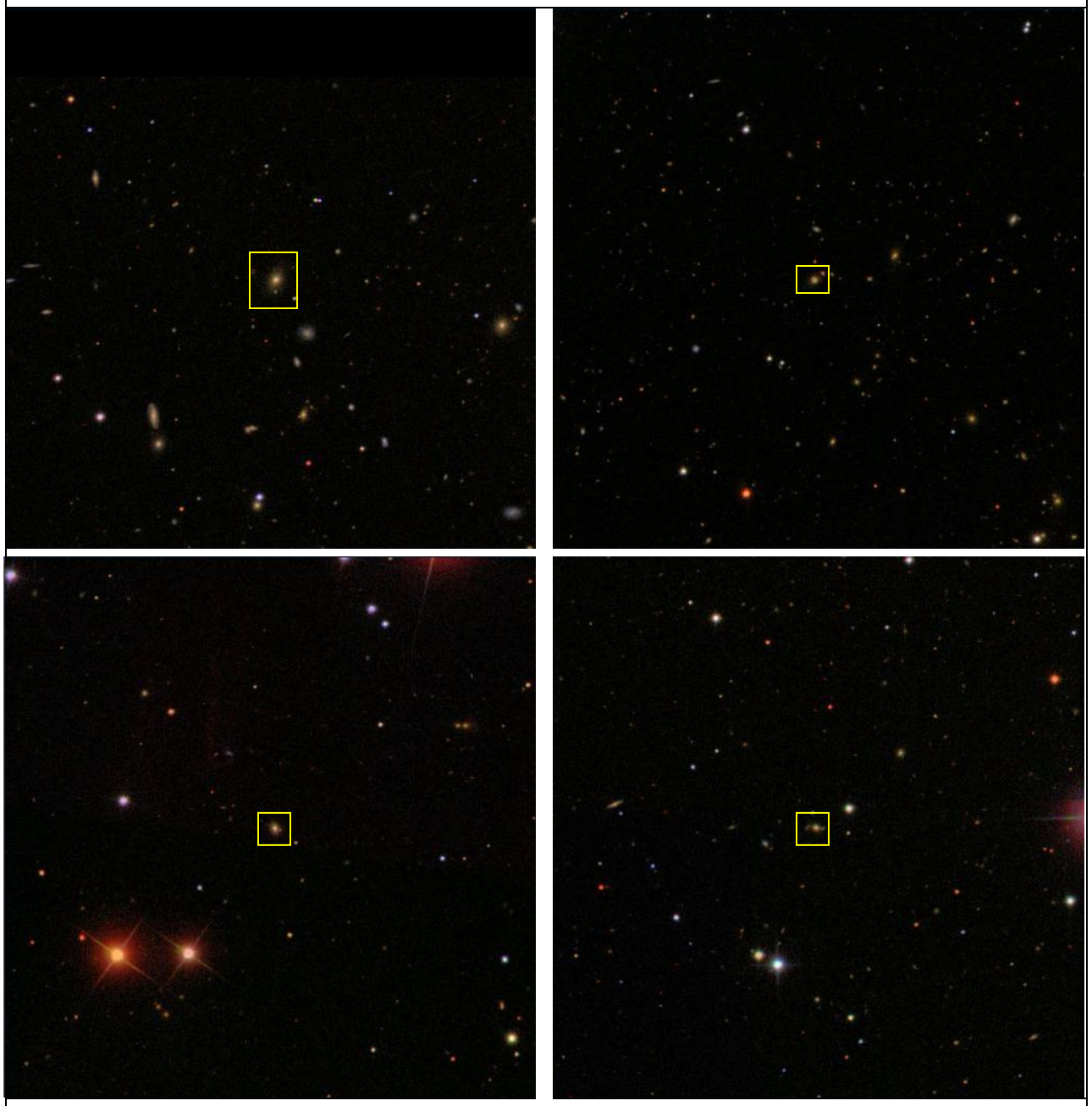

FIGURE 4: The images on the top show galaxies (3) on the left and (32) on the right in relatively dense regions. The gray and yellow fuzzy ovals are galaxies, while the red, white, and blue dots are stars in our own galaxy, which have no impact on the density. Galaxies (5) and (34) are shown in the bottom left and right, respectively. The majority of the objects, including the two bright red bodies on the left of (5), are stars, making this a low density region. These images show that the cylinders are a decent representation of galaxy density.
Photos courtesy of Sloan Digital Sky Survey

The effects of $f(R)$ theories of gravity disappear on the small scale due a proposed chameleon mechanism which is suppressed in areas of higher matter density, like on Earth. While not all galaxies are the same mass, finding a population density of galaxies introduces a way of measuring the environmental matter density relative to other galactic regions.

7. SEARCHING FOR AN ENVIRONMENTAL DEPENDENCE

Checking for the environmental dependence is easy now that all components have been calculated. The result of graphing the mass differences and regional densities can be seen in Figure 5. Taking the mass differences in Section 5 and comparing them to the corresponding population densities of Section 6 reveals a slight dependence, though nothing conclusive. The trend lines are negative, which agree with Zhao et al 2011a. As density increases, the mass difference decreases. Even so, the plots most closely resemble scatter plots, with no real convergence. Reasons for this are discussed in Section 8, but wild variations in the mass percent difference and small number statistics severely hinder the final results.

To confirm these results, 30 galaxies were chosen at random from the sample of 44. The dynamical and lensing mass percent difference was compared to the population density, with new slopes being calculated. This was repeated 99 times to somewhat randomize the samples. The average slope for this test remained the same as the initial set. If the sample set of galaxies chosen for this project is truly representative of galactic populations at that redshift, the randomized slopes seem to confirm the existence of a slight dependence of the mass percent difference on the environmental matter density.

FIGURE5: ENVIRONMENTAL DEPENDENCE

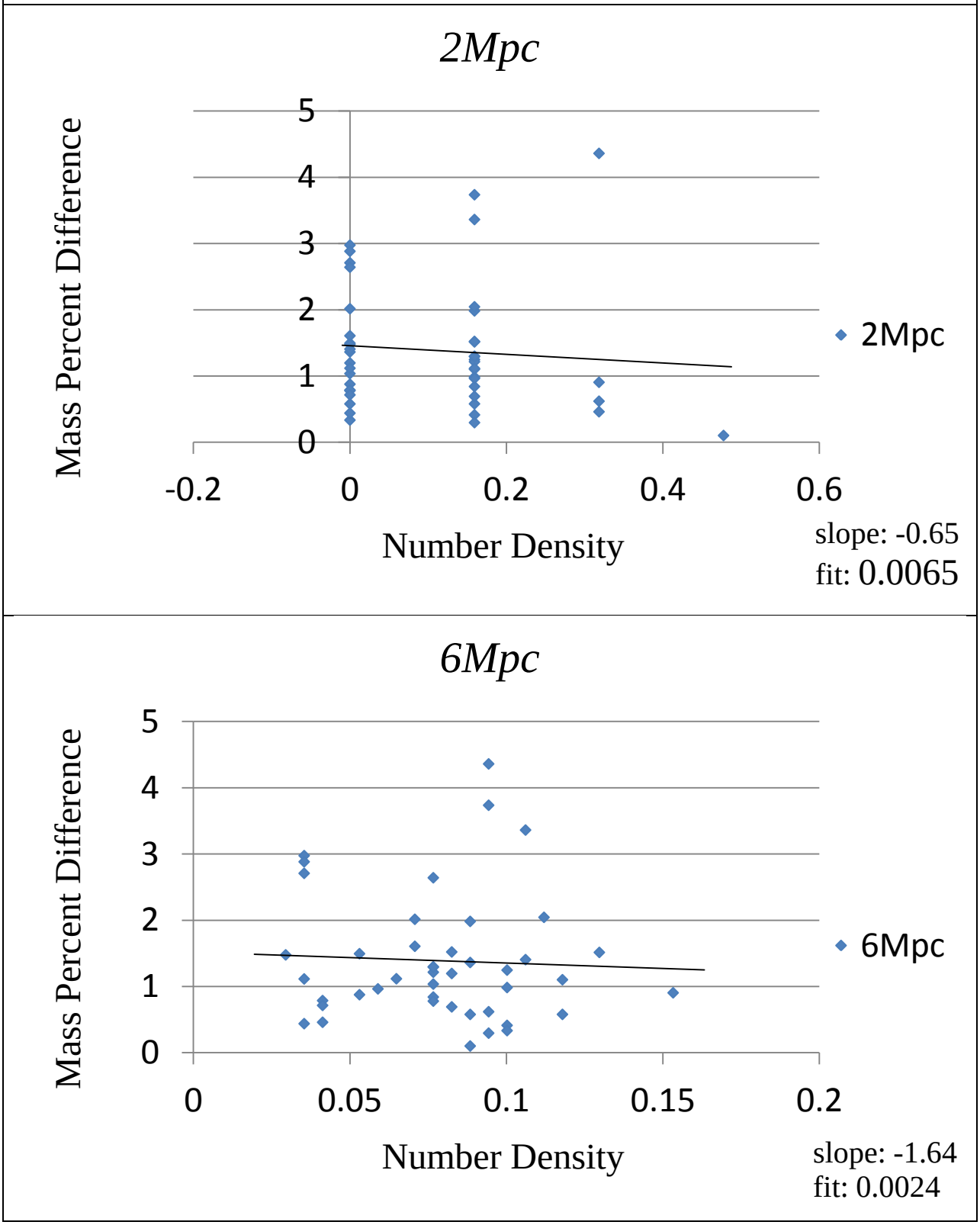

FIGURE5: ENVIRONMENTAL DEPENDENCE (cont.)

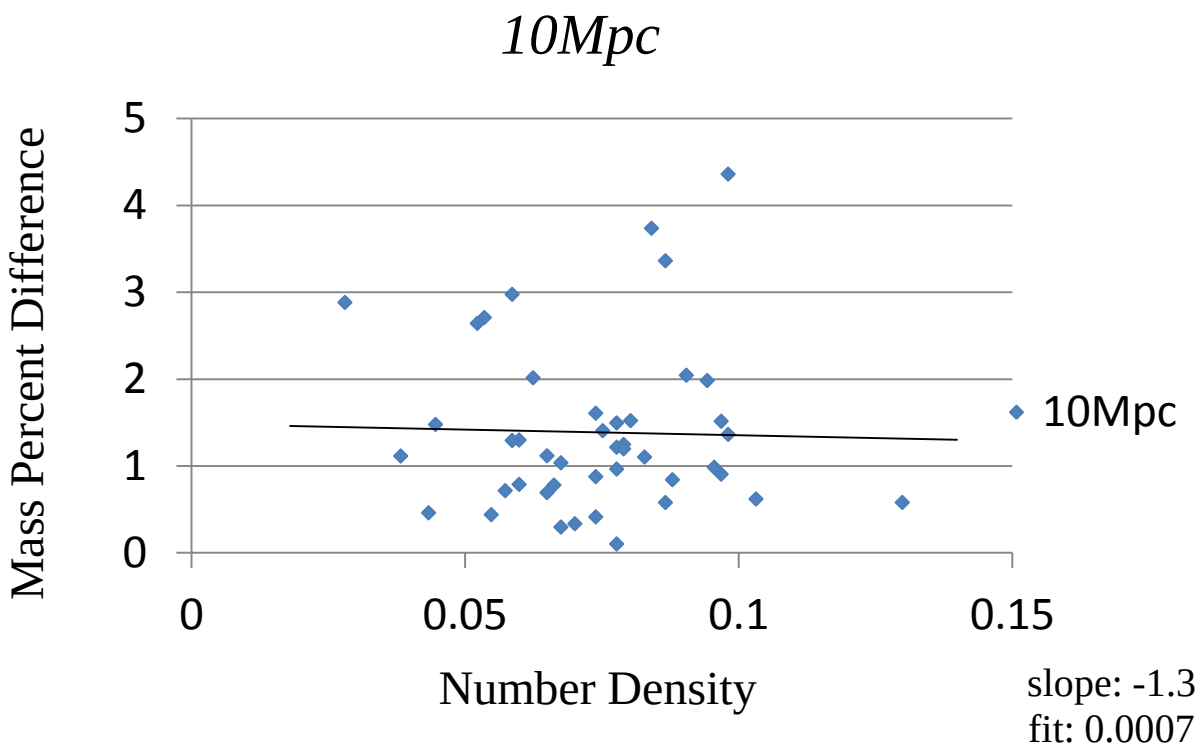

FIGURE 5: This graph shows the relationship between the mass percent difference and the population densities of the region surrounding the sample galaxies using cylinders of 2Mpc, 6Mpc, and 10Mpc diameters. The trend lines have small slopes, and with just visual inspection, the graph looks most like a scatter plot. The lack of a definite trend leads to a null conclusion.

8. FINAL RESULTS

Based on the plots in Figure 5, it is difficult to claim success in either direction. The slopes of the trend lines seem to confirm the theories predicted by modified gravity, though with incredibly weak fits. The coefficients of determination for each of the fit lines were well below 1%. This is in part due to the large variation in percent mass differences found in Section 5, along with the small sample size of 44 galaxies. Due to the large amounts of uncertainty and the lack of convergence, no definitive conclusions can be drawn from the completed research.

9. CONCLUSION

While no definitive answers can be found in the above description, the project was successful in showing that the parameters exist for searching for modified gravity. Better techniques of defining the environment and more accurate models in the mass equations should yield tighter results. The methods presented in this paper were just one combination of several possible techniques. Classifying each individual galaxy and using mass equations that better model the specific galaxy type would better represent the dynamical mass. Using a combination of luminosity and distance parameters may help define a more consistent neighborhood and eliminate the need for the error-prone photometric redshifts. Learning to write more effective queries for data retrieval from the SDSS database also opens new doors. Such queries would allow for finding ways around the maximum data limit that can be downloaded, solving some issues with the nearest neighbor technique prescribed by Zhao et al 2011a and mentioned in Section 6. A much larger sample size may also reveal a stronger correlation. Future work is warranted given the large amount of available data and the potential to test other combinations for determining the masses and environments.

REFERENCES & ACKNOWLEDGEMENTS

Bolton, Adam S. et al. 2008a. *The Sloan Lens Arc Survey V*. (arXiv: 0805.1931v1).

Bolton, Adam S. et al. 2008b. *The Sloan LEN ACS Survey VII*. (arXiv: 0805.1932v1).

Carroll, Bradley W. and Dale A. Ostlie. *An Introduction to Modern Astrophysics*. 2nd ed. San Francisco, CA: Pearson Education, Inc., 2007.

Hartle, James B. *Gravity: An Introduction to Einstein's General Relativity*. San Francisco, CA: Pearson Education, Inc., 2003.

Khoury, Justin and Amanda Weltman. 2004. *Chameleon Cosmology*. (Phys. Rev. D 69, 044026).

Lemonick, Michael D. "Physics Nobel: Why Einstein Was Wrong About Being Wrong." *Time.com*. Time Inc., 5 Oct. 2011. Web. 10 Feb. 2012.

Narayan, Ramesh and Matthias Bartlemann. 2008. *Lectures on Gravitational Lensing*. (arXiv: 9606001v2).

Riess, Adam G., et al. 1998. *Observational Evidence from Supernovae for an Accelerating Universe and a Cosmological Constant*. (arXiv: 9805201v1).

SDSS3.org. Sloan Digital Sky Survey III. <sdss3.org/dr8/>.

Sotiriou, Thomas P. and Valerio Faraoni. 2010. *f(R) Theories of Gravity*. (arXiv: 0805.1726v4).

Sparke, L.S. and J.S. Gallagher III. *Galaxies in the Universe: An Introduction*. 2nd ed. New York: Cambridge University Press, 2007.

Wright, E.L. 2006. A Cosmology Calculator for the World Wide Web. (arXiv: 0609593v2).

Zhao, Gong-Bo, et al. 2011a. *Testing General Relativity Using the Environmental Dependence of Dark Matter Halos*. (arXiv: 1105.0922v3).

Zhao, Gong-Bo, et al. 2011b. N-body simulations for fðRÞ gravity using a self-adaptive particle-mesh code. (PhysRev D 83, 044007).

Special acknowledgements go to the Institute of Cosmology and Gravitation at the University of Portsmouth in Portsmouth, UK where a majority of this work was completed. Special thanks to the Etscorn family, the University of Louisville Honors Department, and Dr. Blaine Hudson, Dean of Arts and Science, University of Louisville for their financial contributions.

Also, thanks to Dr. James Lauroesch and Dr. Robert Nichol for their advice and guidance.

APPENDIX A: COMMON DEFINITIONS

Angular Diameter Distance: This representation of physical distance is found by dividing the actual size of an object by the angle it subtends (Carroll & Ostlie 2007).

Arcsecond: With 360° in a circle, an arcsecond is $1/3600^{th}$ of a degree and denoted by "

Line of Sight: The line of sight is an imaginary line extending straight out from an observer on Earth.

Luminosity Distance: The luminosity distance is a function of luminosity and flux, and is best used at small redshifts (Carroll & Ostlie 2007).

Parsec: A parsec is a unit of distance measured when 1 arcsecond is subtended by 1 astronomical unit, which is defined as the distance between the Earth and Sun.

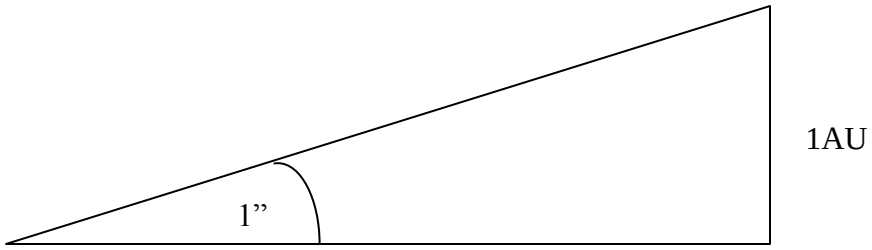

1 parsec

Redshift: The expansion of the universe causes light to be stretched as it travels through spacetime. The wavelengths increase as a result, "reddening" the light. Redshift is often used as both a conceptual measure of time and distance.

Solar Mass = $2 \times 10^{30} kg$ and denoted by $M_{\odot}$ (Sparke & Gallagher 2007)

Velocity Dispersion: The velocity dispersion is a general measure of the motions of stars within a galaxy. These are measured spectroscopically by looking for Doppler shifts in the light coming from stars as they rotate around the galaxy (Carroll & Ostlie 2007).